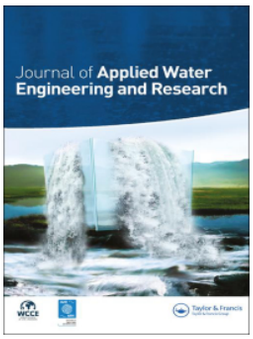

Journal of Applied Water Engineering and Research

ISSN: 2324-9676 (Online) Journal homepage: www.tandfonline.com/journals/tjaw20

Optimising woody debris dam design for flood risk management

David Furnues, Judith R. Cudden & Matthew McParland

To cite this article: David Furnues, Judith R. Cudden & Matthew McParland (05 Mar 2026): Optimising woody debris dam design for flood risk management, Journal of Applied Water Engineering and Research, DOI: 10.1080/23249676.2026.2637536

To link to this article: https://doi.org/10.1080/23249676.2026.2637536

Published online: 05 Mar 2026.

JOURNAL OF APPLIED WATER ENGINEERING AND RESEARCH
https://doi.org/10.1080/23249676.2026.2637536

Taylor & Francis
Taylor & Francis Group

Optimising woody debris dam design for flood risk management

David Furnues[a], Judith R. Cudden[b] and Matthew McParland[b]

[a]Hydro-environmental Research Centre, School of Engineering, Cardiff University, Wales, UK; [b]Jacobs, Leeds, UK

ABSTRACT

This study examines how variations in engineered woody debris dam designs affect bed morphology. Pools and riffles, formed by these dams, create varied flow velocities and depths, dissipating energy and mitigating downstream flood risk. Understanding their hydraulic effects on scour and deposition remains limited. Laboratory flume experiments were conducted at two discharges, using two structure designs, each comprising three wooden cylinders with varying bed-to-base gaps. Digital Elevation Models were generated using a Kinect v1.0 and Matlab. To verify localised velocities and bed shear stress values, a computational flume was constructed using Jacobs Flood Modeller. Findings showed that the 2D model replicated the physical experiments effectively, highlighting increased bed shear stress downstream of the structure and corroborating the location of maximum scour depth. Results indicated that structures close to the bed increased scour depth beneath them, enlarging the wetted area and reducing their effectiveness in slowing the flow.

ARTICLE HISTORY
Received 14 August 2024
Accepted 23 February 2026

KEYWORDS
Woody debris dams; geomorphic change; flume experiments; Natural Flood Management; computational modelling; Flood Modeller

Introduction

The Intergovernmental Panel on Climate Change (IPCC) states, with high confidence, there will be increasing extreme precipitation in Europe which will substantially increase river flood risk (Kovats et al. 2014). Extreme rainfall saturates the soil, preventing infiltration and increasing surface runoff, which accelerates fluvial flooding. Urbanisation, with impermeable infrastructure like roads and car parks, further exacerbates rapid runoff and higher peak discharge.

The IPCC supports Natural Flood Management (NFM) using techniques like afforestation and instream wood reintroduction. It also advocates better agricultural practices to reduce erosion and controlled flooding of agricultural land to mitigate urban flooding (Jiménez Cisneros et al. 2014). These measures aim to restore natural catchment processes and reduce surface runoff, releasing it slowly to attenuate downstream flood peaks. However, there is uncertainty about the efficacy of NFM, such as the impact of woody debris dams, due to limited scientific evidence (Dadson et al. 2017; Wingfield et al. 2019). Woody debris dams are one such NFM technique designed to function as in-channel Runoff Attenuation Features (RAFs) in upper agriculture catchments. This paper addresses the IPCC's challenge of implementing effective NFM at the catchment scale by investigating the effectiveness of instream woody debris dams in promoting natural processes.

Engineered woody debris dams replicate natural dams formed by fallen trees and branches (Leakey et al. 2020). They slow flow, increase temporary water storage, and enhance channel-floodplain connectivity, enabling greater time for infiltration and percolation, thus attenuating the flow for managing downstream floods (Ngai et al. 2017). They also impact on channel morphology by altering flow patterns, increasing flow resistance, and creating backwater effects (McParland 2021; Furnues 2023). Despite extensive use, there remains limited understanding of their hydraulic effects on channel bathymetry, which can be used to the benefit of flood risk, but can induce adverse effects (Pearson 2020).

Pools and riffles contribute to hydraulic complexity with pools being deep areas of low velocity and riffles exhibiting higher hydraulic gradients and faster velocities, particularly at low discharge. At high discharge, riffles increase bed roughness and hence slow the flow (Obach 2011). Their alternating pattern reduces channel erosion and enhances stability. Pool-riffle sequences are linked to meander development, which lengthens the channel, decreasing channel slope and velocity (Whitten and Brooks 1972). Despite creating fast, turbulent water, riffles form depositional zones that

CONTACT David Furnues David23.F@outlook.com Hydro-environmental Research Centre, School of Engineering, Cardiff University, Wales, UK

reinforce the channel bed, while pools create natural barriers. Variation in the channel morphology, created by woody debris dams, can dissipate energy altering flood frequency distribution (Nunnally 1978).

Numerous studies have investigated the mechanisms by which obstruction-related pools are formed. Beschta (1983) researched the effects of single horizontal cylinders on scour depth as a function of cylinder diameter, position above the bed and flume discharge. Discharge below obstructions lying on the bed was an important scouring mechanism along with larger obstructions which enabled deeper scour. Other researchers have investigated single cylinder effects on scour depths, oriented upstream and downstream (Cherry and Beschta 1989; Svoboda and Russell 2011). Experimental work on single cylinders has given insight into the hydraulic and geomorphic effects of individual key members. Rather than deploying simple designs composed of single solid cylinders, this study represents woody debris dams as multiple horizontal cylinders with vertical spacings between them, set at different elevations above the bed.

Understanding the influence of woody debris dams on channel morphology is critical to developing an insight into the mechanisms that can reduce flood magnitude downstream. Though the natural form of woody debris dams is complex, they contain basic components of simplified shapes that can be used in flume experiments to improve understanding of their effects on bed morphology (Thompson and McCarrick 2010). The aim of this study is to address the research gap targeting the need for a better understanding of the effectiveness of structural design and condition on sediment transport dynamics (Ngai et al. 2017). The objectives are to assess the impact of different woody debris dam structures on channel bathymetric evolution in a controlled laboratory flume to inform structural design criteria and to use a 2D computational model to simulate channel hydraulics in the vicinity of the structural design and validate local velocity and bed shear stress distributions.

Method

Experimental setup

Experiments were conducted, at Cardiff University, in a recirculating flume with dimensions of 10 m in length, 1.2 m in width and 0.3 m in depth. Two PVC sections, each measuring 10 × 0.3 × 0.225 m, were installed to form a 0.6 m-wide channel with floodplains. This setup allowed for two flow conditions: 100% bankfull discharge (100% Q_{bf}) in Series A, and 80% bankfull discharge (80% Q_{bf}) in Series B. The sediment bed height was levelled at 75 mm (Figure 1), and Series 1 was repeated three times and Series 2, twice.

The present study was appropriately scaled to match other research, using similar-sized experimental setups to enhance experimental reliability. For example, Penna et al. (2020) used a flume that was 9.6 m long and 0.485 m wide, with a single cylinder diameter (Di) of 30 mm placed at the centre. Beebe (2000) used a flume that was 10 m long and 0.63 m wide, with a single cylinder of Di = 63 mm placed 6 m upstream of the tailgate.

Two simplified structures each consisting of three horizontal logs, referred to as cylinders (Figure 2) were inserted 4.74 m upstream of the tailgate. Structures were installed for their respective test runs. Each cylinder had a diameter (Di) of 25 mm, spanning the width of the main channel of 0.6 m.

Two types of structures were designed and tested to investigate their impact on bathymetric evolution. Structure 2 was an inverted structure 1. The vertical spacing between cylinders (G) was maintained at 10 mm or 0.4Di. Structure 1 had its base cylinder on the bed (e = 0), while structure 2 had its base cylinder raised above the bed (e = 35 mm or e = 1.4Di), where e is the depth of the bottom of the structure to the bed. Both structures had the same blockage area (0.045 m⊃2), but blockage ratio varied with discharge (0.5 and 0.58 at 100/80% Q_{bf}, respectively). All structures were fully submerged. The gap ratio between the base cylinder and the bed was referred to as e/Di (Yang et al. 2019).

Before the structure was inserted, the flow conditions for the experiments were distinctly characterised by varying discharge rates, mean velocities, and wetted areas for Series A and Series B. Series A displayed a mean velocity of 0.244 m/s, a discharge of 0.022 m^3/s, and a wetted area of 0.09 m^2. In comparison, Series B had a mean velocity of 0.222 m/s, a discharge of 0.018 m^3/s, and a wetted area of 0.078 m^2. These flow conditions were set to ensure that, once the structure was inserted, the bed shear stress values could be comparable to other studies.

A Nixon Tecfluid Flowmeter Model CU100 (accuracy: ±1.5% of the reading value), installed in the flume, measured the discharge. A Nortek Vectrino ADV (accuracy: ±1 mm/s) was positioned 2.2 m upstream of the tail gate, at a height of 0.37 × he flow depth above the bed. For bed and water surface profiling, a Vernier point gauge (accuracy: ±0.1 mm) (Sankar 2015) and Kinect v1, were mounted above the

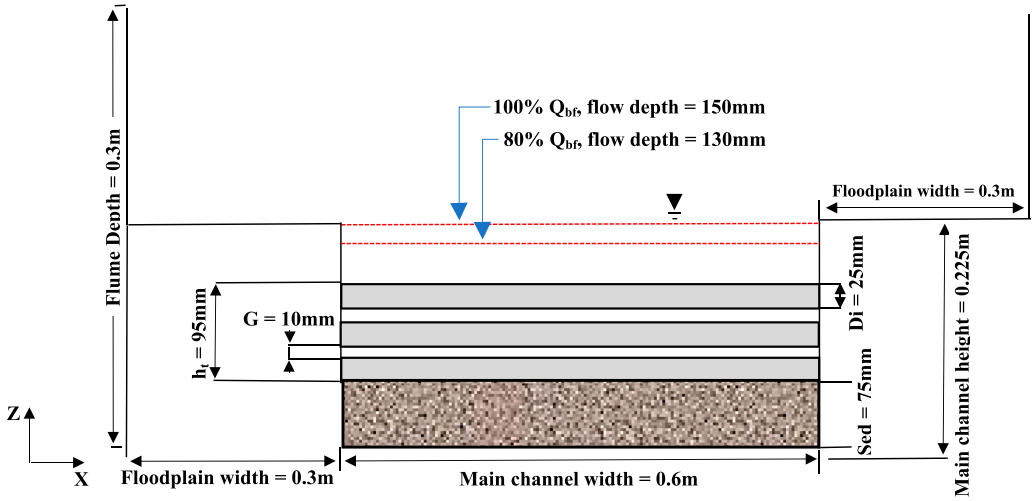

Figure 1. Series 1A/B setup: Three cylinders with a diameter (Di) of 25 mm, sediment height (Sed) of 75 mm, base-to-bed depth (e) of 0 mm, vertical spacing between cylinders (G) of 10 mm and maximum height of structure above the bed (h_t) of 95 mm. Main channel height of 0.225 m, main channel width of 0.6 m. Flow depth at 100% Q_{bf} of 150 mm and at 80% Q_{bf} of 130 mm. Flume width of 1.2 m, with two 0.3 m floodplain widths. Adapted from Furnues, (2023).

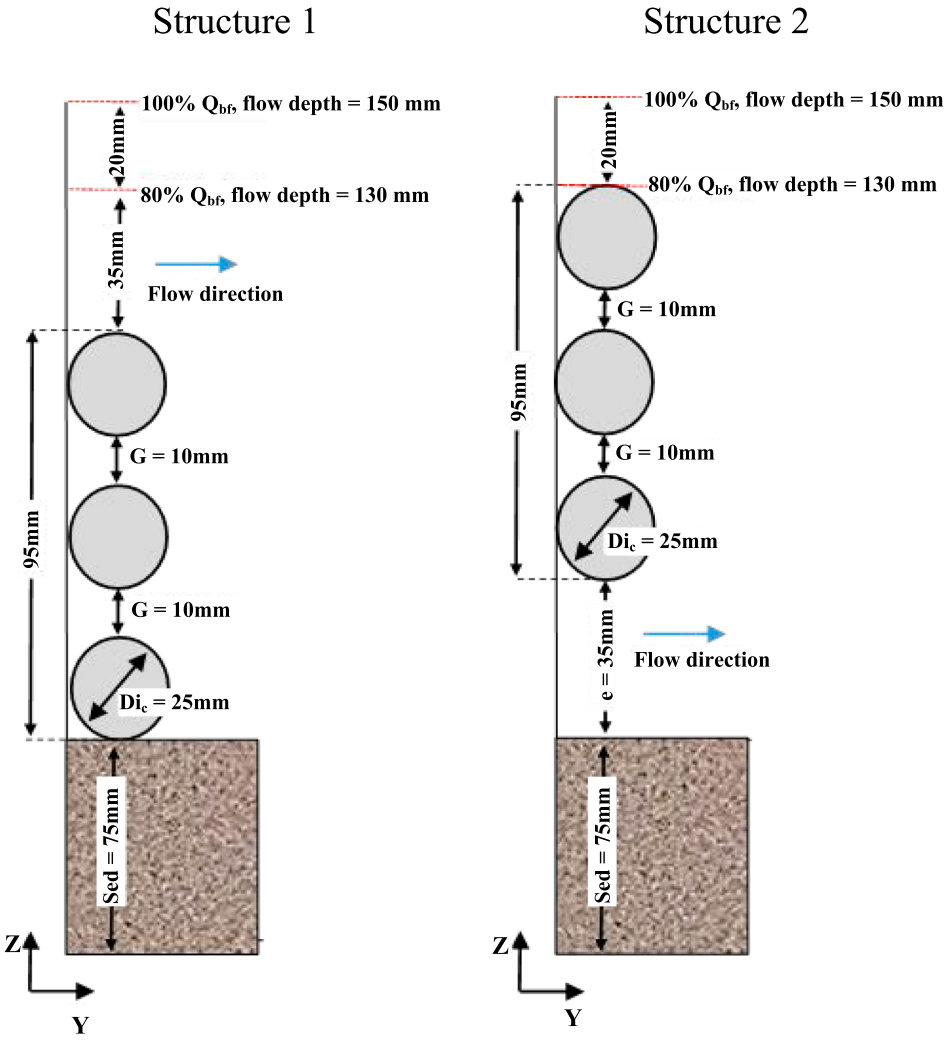

Figure 2. Conceptual diagram of single column vertical stack designs and dimensional criteria for the experimental Series. The Z-axis represents depth, while the Y-axis denotes flume length. Series A is 100% Q_{bf} and Series B is 80% Q_{bf}. and structures are numbered 1 and 2. Adapted from Furnues, (2023).

flume on a carriage to measure bathymetric change. Structure location, particle size and structure blockage ratio remained constant. Structure design (Series 1 and 2) and discharge (Series A and B) varied between experiments.

Sediment and flow conditions

All experiments were conducted in clear water conditions. Sediment size was calculated using the critical tractive force method and verified using the competent velocity approach. Particle size was identified just below the threshold of motion at 1 mm. Experiments were carried out using grain size 1–2 mm with a sediment distribution of 52% being in the range 1–1.18 mm. Prior to each experiment, the bed was manually levelled with a surface slope of 0.001 m/m. A surface water energy slope graph was constructed at both discharges to establish uniform flow conditions. On structure insertion, flow depth and longitudinal water surface profile were impacted with the disruption of uniform flow conditions and flow regime continuity.

The bed morphology survey was carried out at the end of the Run after the channel was fully drained. Once experimental Runs were completed, the pumps were gradually shut down and the water slowly drained to maintain the integrity of the channel morphology. The Kinect in conjunction with Matlab Image Acquisition enabled creation of Digital Elevation Models (DEMs) of the bed morphology. To identify errors and validate the point cloud image acquisition of the dry bed, a point gauge was used.

A graphical solution was applied to construct non-parametric regression functions for estimating local scour depth from established datum prior to flow conditions to the bed (d_s) and the depth of scour at equilibrium (d_{se}) with the influence of discharge. Time to equilibrium and experimental shut down were determined at the point of plateau. Point of plateau is defined as when the reduction of scour rate is < 0.05Di within 24 hrs. A time-dependent analysis was performed where all Runs were shut down at 96 hrs to ensure experimental consistency, which enabled comparison of bathymetric evolution at a fixed time.

Kinect calibration

Kinect calibration refers to the mapping from raw digital number to real world, x, y, z points (Mankoff and Russo 2013). An external calibration procedure obtained the Kinect horizontal and vertical spatial resolutions. The Kinect was positioned perpendicular from a planar surface spanning the full Field of Vision (Khoshelham and Elberink 2012). Once appropriate spatial resolution was obtained, future point cloud spatial resolutions could be quantified.

Kinect depth accuracy is the difference between the appropriate true measured distance from Kinect to principal point (Z_{bs}) compared to the digital measured distance (Mankoff and Russo 2013). A point cloud of the planar surface provided the digital numbers to obtain the digital distance. At $Z_{bs} = 1$ m depth accuracy error was calculated at 0.1% or 1.03 mm. Precision is defined as the spread of measurements around the mean and is also repeatable under unchanged conditions (Mankoff and Russo 2013). Depth resolution is the step-sized deviation [$q(Z_{bs})$] from the depth accuracy and the smallest measured distance between points repeatable under unchanged conditions. Depth resolution is determined by the digital numbers used with the Kinect (Khoshelham and Elberink 2012). For the present study, $q(Z_{bs}) \approx 3$ mm when $Z_{bs} = 1$ m (1). (m_p/fb_1) was pre-determined at $2.85e^{-5}$ by Khoshelham and Elberink (2012).

$$q(Z_{bs}) = \left(\frac{m_p}{fb_1}\right) {Z_{bs}}^2 \tag{1}$$

To calibrate for common correspondence, lens distortion and de-centring, least square adjustment algorithms were applied (Li 2018) (2), where x and y are the ideal coordinates, xd and yd are the corresponding coordinates and k… denoting radial distortion coefficients, while r… corresponds to the square root of the sum of x… or y… ideal coordinates.

$$\begin{aligned} x_d &= x(1 + k_1 r^2 + k_2 r^4 + k_3 r^6) \\ y_d &= y(1 + k_1 r^2 + k_2 r^4 + k_3 r^6) \\ where: r &= \sqrt{x^2 + y^2} \\ x_d &= x(1 + k_1 r^2 + k_2 r^4 + k_3 r^6) \end{aligned}$$

Velocity verification via hydro-environmental modelling

Flood Modeller v6.1. (FM) was used to construct a 2D computational flume with channel characteristics replicating the flume experiment. A computational flume enabled localised velocity readings and bed shear stress spatial distributions to be captured without being intrusive to the flow regime, which could have disturbed channel bathymetry.

Firstly, to simulate the flume channel, a matrix was constructed using Microsoft Excel 365, where computational flume spatial resolution was set to 0.05 m. As FM, 2D simulations cannot represent vertical gaps between key members, woody debris dam blockage

area was simulated in FM. Series 1A/B flume structure, with its base cylinder on the bed, was simulated by increasing the bed elevation at the structure location. Once the matrix was constructed with the heightened bed representing the structure, it was then imported into ArcGIS Pro 2.9.0 before a Digital Elevation Model (DEM) was constructed.

The DEM was then imported into FM, where the computational area and active area were drawn around the area of interest. Channel inflow and outflow were derived by drawing boundary lines at upstream inflow and downstream outflow. To run the simulation with the same flow conditions as the flume experiment, a new 2D simulation was constructed. Relevant layers were inserted into the required field tabs. Depending upon which Series was being represented in the simulation, the constant discharge value was altered between 0.022 m^3/s (Series A) and 0.018 m^3/s (Series B).

Results and discussion

Scour evolution

To determine when the depth of scour at equilibrium (d_{se}) was reached, the time to equilibrium was established. At first, the insertion of the structure restricted the hydraulic radius, causing scour to increase rapidly over time before slowing, with sediment transport rates starting to plateau (Figure 3). Experimental data indicated $\approx$50% of the equilibrium scour depth ($0.5d_{se}$) was attained in a time $\leq$ 10% of the time to equilibrium, depending on discharge.

Sediment motion was initiated when the bed shear stress exceeded the critical shear stress. Initially, sediment scour occurred at a higher Shield's parameter dimensionless ($\tau*$) of 0.13 for Series A and 0.118 for Series B, before decreasing until equilibrium scour depth was reached and the bed re-stabilised. Typically, $\tau*$ values range from 0.025 to 0.8, depending on the relative density (Berenbrock and Trammer 2008). Findings were comparable to similar studies (Lee et al. 2018 at $\tau* = 0.15$ and Gao et al. 2006 at $\tau* = 0.25$).

The structure altered localised velocities and restricted the hydraulic radius, controlling sediment entrainment. Scouring continued as localised velocities remained above the critical velocities, slowing only as the scour depth increased and the rate of entrainment diminished until equilibrium was achieved (Tammela et al. 2010).

Discharge influenced scour depth by increasing flow velocity and bed shear stress, which led to greater sediment entrainment and deeper scour holes. Chiew and Melville (1987) and Melville and Sutherland (1988) found that higher flow rates caused more significant scour around structures. In Series 1A Run 3, the maximum scour depth (d_{smax}) reached 61 mm, compared to 40.1 mm in Series 1B Run 3. Series B showed a smaller d_{smax} variance (5 mm) than Series A (14 mm), indicating that lower discharge results in less variance (Figure 3). At lower discharges, bed shear stress remained closer to the critical tractive force, reducing variance between Runs.

To achieve d_{se} it was necessary to run experiments for 72 hrs (Series A) and 48 hrs (Series B). These extended periods enabled observation of sediment transport processes and ensured that the system reached a true state of scour equilibrium. In contrast, experiments with shorter durations of 12 hrs, for which the time to equilibrium is 48 hrs, would have only achieved $\approx$65% of the true d_{se} (Series 1B, Run 2). This finding displays the importance of prolonged experimental durations to capture the scouring process.

Bathymetric evolution over shorter timescales was analysed by shutting down Series 1A, Run 3 and 1B, Run 2 every 12 hrs, while Series 2A, Run 1 was shut down every 24 hrs (Figure 3). All Runs were shut down at 96 hrs past the time to equilibrium to ensure experimental consistency between Runs.

As well as discharge governing time to equilibrium, the depth of the bottom of the structure to the bed (e) also proved an important factor affecting d_s. When $e = 0$, the hydraulic restriction increased shear velocity and generated a pressure difference that forced the flow underneath, known as seepage flow (Fredsøe 2016). This mechanism triggered downstream scouring, followed by tunnel erosion being driven by a jet flow drawn beneath the structure (Lee et al. 2018). In this way, a deeper and larger scour hole developed increasing the flow intensity and entrainment with bed shear stress exceeding critical tractive force. This process took longer for the scour rate to reach the depth of scour at equilibrium for $e = 0$ in comparison to $e > 0$. As e increased, the rate of scour decreased, and equilibrium was reached more quickly.

Temporal development of deposition

Centreline longitudinal bed profiles display scour evolution and exit dune extent past time to equilibrium until 96 hrs (Figure 4). Though d_{se} was reached at 72 hrs (Series A) bed morphology continued to develop with the exit dune extending further downstream. Even after the local scour depth stabilised, sediment particles continued to be dislodged and were transported downstream. Another reason for the extension of the exit dune after equilibrium is that variations in localised

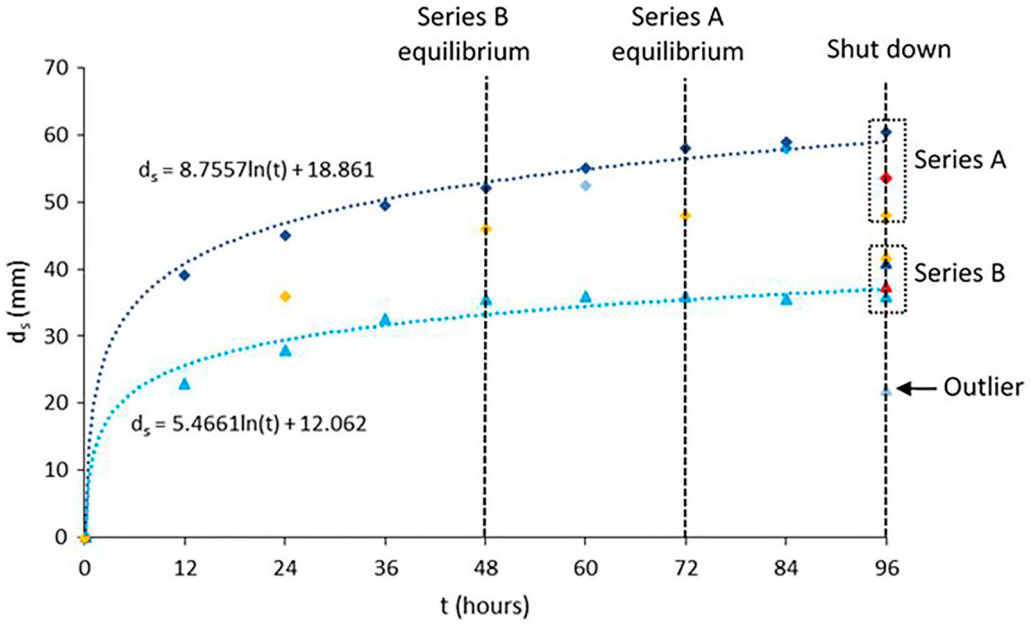

Runs	Series			
1	◆ 1A	▲ 1B	◆ 2A	▲ 2B
2	◆ 1A	▲ 1B	◆ 2A	▲ 2B
3	◆ 1A	▲ 1B		

Figure 3. This time-dependent analysis shows scour depth evolution in clear water conditions. The scour depth is asymptotic, with threshold criteria marked by negligible changes in scour development. This threshold, where the scour rate plateaus, ensures consistent development across all Series. The image shows the time taken for experiments to reach equilibrium. Adapted from Furnues, (2023).

velocity and turbulence downstream contributed to the redistribution and deposition of sediment particles. This displays the dynamic nature of sediment transport, where localised equilibrium does not necessarily imply a cessation of sediment movement in the system. For instance, Figure 4 shows d_s continued to deepen from 51.7–58–61 mm and the exit dune continued to extend downstream from a longitudinal distance of 526–830–947 mm from 60–84–96 hrs (Series 1A, Run 1/2/3). Though as aforementioned, experimental shut down was set at 96 hrs to ensure experimental consistency between Runs.

Scour initiated $\approx$30 mm upstream of the structure, which developed into tunnel erosion. The maximum depth of scour began upstream and progressively moved downstream, with bed shear stress dropping below critical tractive force. Sediment was deposited downstream of the scour hole forming an exit dune, which lengthened and flattened over time. Beschta (1983) validates discharge controls scour and depositional features.

Series 1A, Run 1 had a steeper angle of repose and decline either side of the exit dune crest, compared to Series 1A, Run 2 and 3 (Figure 4). At Series 1A, Run 2 and 3, the maximum height of the exit dune slightly increased from Series 1A, Run 1. As the exit dune developed downstream, the angle of repose decreased.

Bed profiling

Series A had the exit dunes developing further downstream than Series B (Figure 5). Series A, exit dunes appeared wider with a larger areal extent than Series B. Higher discharge created deeper and wider scour with the exit dune moving further downstream. Structures with vertical spacings between cylinders and a base cylinder on the bed generated greater downstream vortices, enhancing turbulence and sediment transport, particularly noted in Series 1A. These observations confirmed that turbulence plays a major role in the entrainment and scouring process.

At high discharge, the structure constricting the channel caused turbulence, increasing local velocities and sediment entrainment. Reduced kinetic energy at lower discharge (100% Q_{bf}: 29.71 J compared to 80% Q_{bf}: 24.59 J) resulted in less sediment entrainment. As

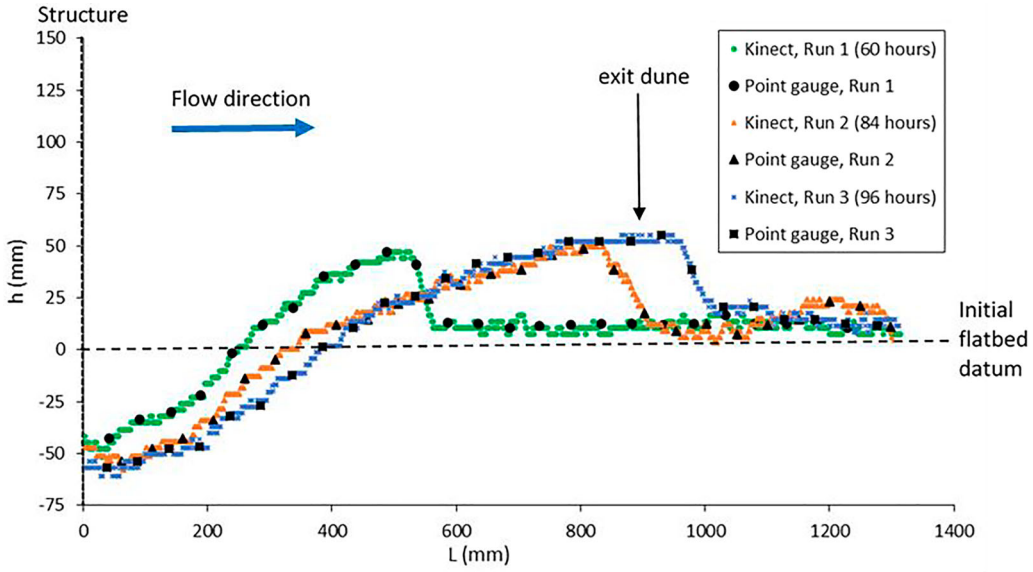

Figure 4. Centreline longitudinal profiles for Series 1A (e = 0). Three Runs were carried out at 60, 84, and 96 h. To validate the results, Kinect depth measurements were compared to those using the point gauge. Adapted from Furnues, (2023).

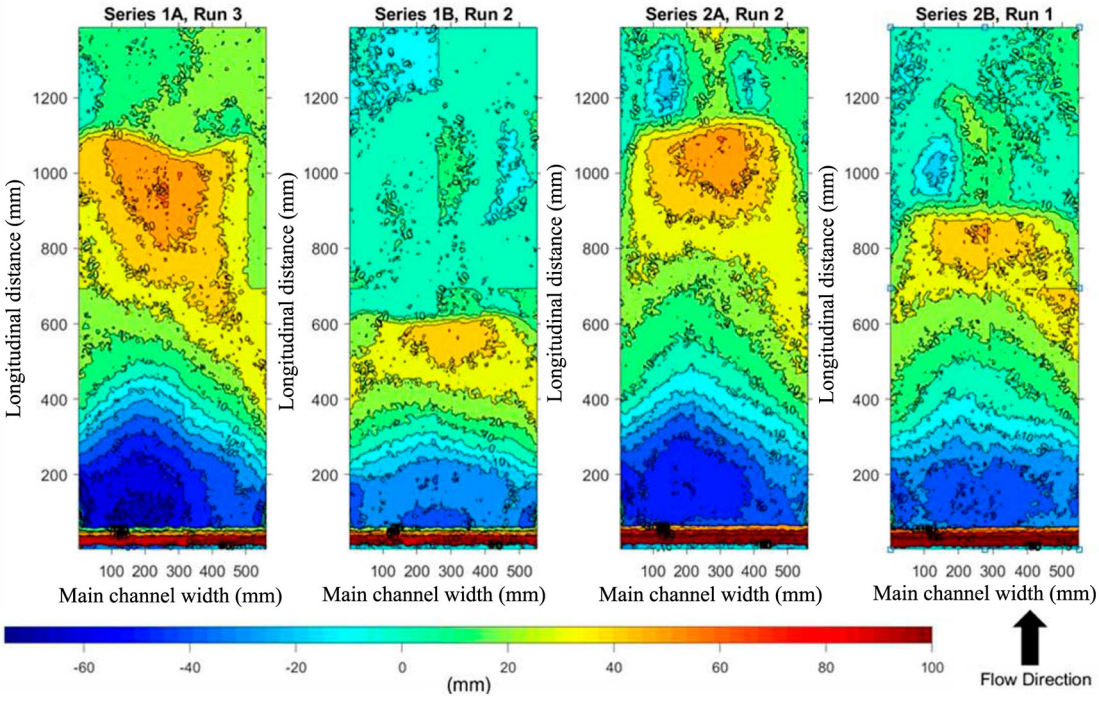

Figure 5. Digital Elevation Models (DEMs) of Series 1–2 (100% and 80% Q_{bf}) show scour and depositional build-up in clear water. Bed topography contours are at 10 mm intervals, referenced to a 1 m fixed datum. The focus is on a longitudinal distance of 1.35 m. Adapted from Furnues, (2023).

aforementioned in the time to equilibrium section, discharge also impacted scour depth by increasing flow velocity and bed shear stress distribution.

This is further illustrated in the comparison between Series 1B and Series 2B. Series 2B, Run 1 had a greater maximum depth of scour (d_{smax}) than Series 1B, Run 2 (Figure 3 and 5). However, Series 1B, Run 1 had greater d_{smax} than Series 2B, Run 2 (Figure 3). Series 1B and 2B d_{smax} remained relatively constant with little variance in which of Series 1B or 2B scoured the most. Beschta (1983) states that when structures have $e > 0$, d_s increases until the initiation of structural overtopping. Series 2B had the top cylinder positioned at the surface with no overtopping, while Series 1B had overtopping, which dissipated energy and reduced the depth of scour at equilibrium. Tammela et al. (2010)

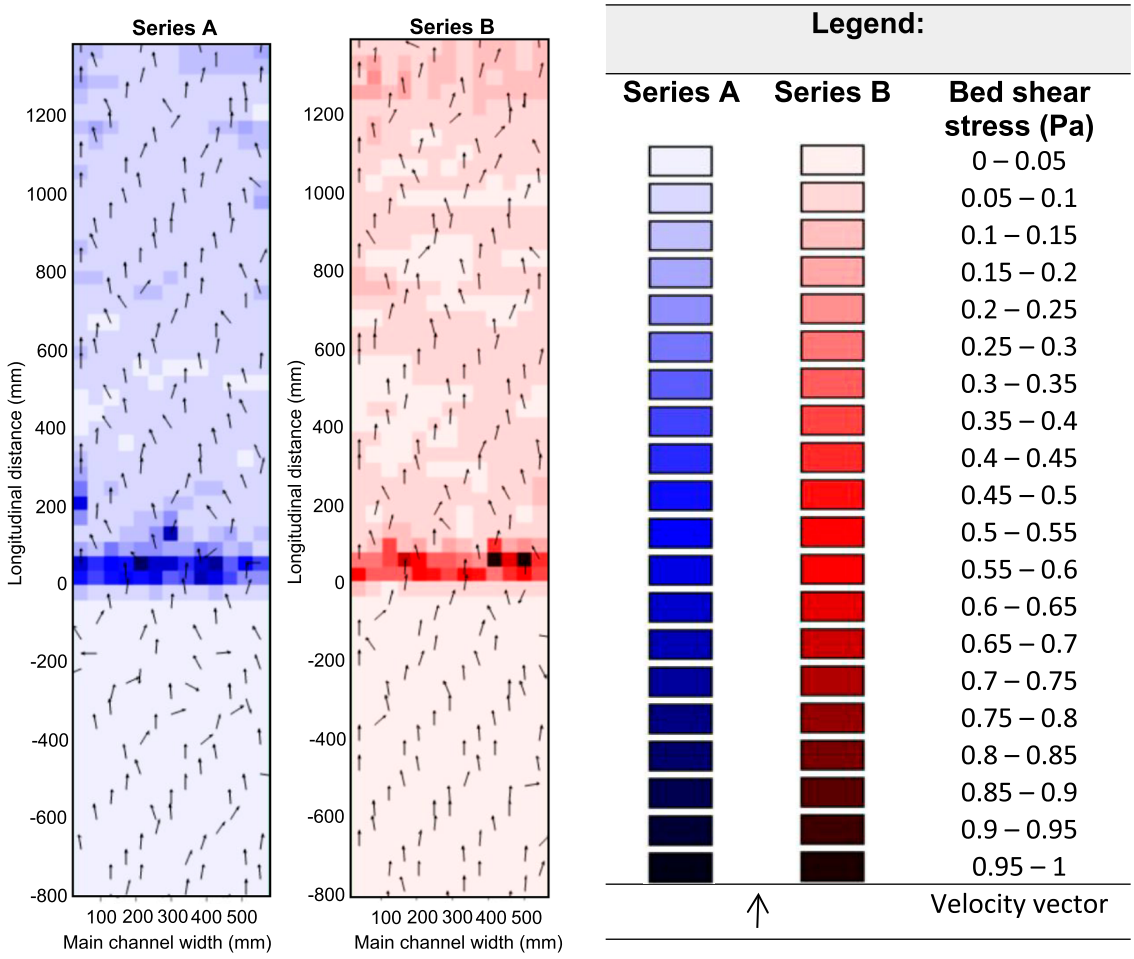

Figure 6. Series A and Series B obstructed channel showing bed shear stress spatial distribution with velocity vectors. The same distance downstream of the structure was examined for comparison to the flume experiments. Adapted from Furnues, (2023).

found that the entire flow should be diverted under the structure for maximum scour depth with spacings in the structure reducing scour efficiency.

The maximum height of the exit dune was near or on the centreline. Exit dunes do not extend at a uniform height over the entire channel width. Series 1B and 2B, showed a different spatial pattern compared to Series 1A and 2A as they exhibited a blunter scour boundary that does not extend as far downstream. At 80% Q_{bf}, exit dunes were smaller and closer to the scour hole with steeper angle of repose towards the exit dunes. Spatial variations in exit dune development could be caused by channel banks creating friction, reducing shear velocity and therefore entraining less sediment.

Both structures had considerable control over the channel morphology in generating pools and riffles (Figure 5). Series 2A and 2B, with e = 1.4Di had maximum depth of scour (d_{smax}) moved further downstream from beneath the structure than Series 1A and 1B (e = 0). This can be explained by Structure 2 allowing the flow to pass freely through the gap under the base cylinder, causing less disturbance to the bed. Series 1A generated turbulence with strong vortex interactions. Series 2B raised above the bed experienced higher throughflows and lower velocities, with weaker vortex interactions.

Flood modelling

2D simulations accurately depicted bed shear stress at the structure at the beginning of the flume experiments, showing an increased bed shear stress immediately downstream of the structure along the centreline. This supports the flume experiment where the deepest maximum depth of scour (d_{smax}) value occurred immediately downstream of the structure. The computational model indicated a flow regime change when the structure was inserted. Upstream of the structure, between – 800 and – 400 mm, streamlines were set on a structured trajectory but closer to the structure at – 400 mm backwater effects were induced and the streamlines began to

deviate off the structured course. Computational models have difficulty in representing flow discontinuity at structures, representing what the models assume as mixing, as grid scale oscillation (Falconer 1986) as seen in Figure 6 from −400 mm upstream of the structure to ≈800 mm downstream.

A limitation within FM is the lack of a standardised unit to replicate the complex matrices of woody debris dams. In the flume experiment, the structure was constructed with three cylinders, causing flow separation around them. However, FM does not have a unit to replicate the spacings between horizontal cylinders. Therefore, the blockage area was simulated by raising the channel bed to replicate channel blockage. Future models with more complex hydraulic units could better replicate intricate structural designs, enabling a more accurate representation of flow dynamics.

Conclusion

This study examines how various woody debris dam structures affect channel bathymetric evolution, to improve structural design criteria. Additionally, a 2D computational model simulates channel hydraulics around the structural design to validate local velocity and bed shear stress distributions. The investigation puts forward design criteria for woody debris dams by capturing scouring potential according to gap ratio between the base cylinder and the bed, leading to better design and greater effectiveness in helping to slow the flow.

Findings show that discharge positively equates to the depth and length of scour, with Series A having a greater d_s compared to Series B. Increased discharge also results in the exit dune having a greater maximum height and being located further downstream of the structure. This finding was supported by 2D FM simulations, which showed that as discharge increased so did bed shear stress. Greater bathymetric changes between the structural designs occurred at higher discharge.

Structures with the base cylinder above the bed ($e > 0$) have the maximum depth of scour located further downstream in comparison to structures with the base cylinder on the bed ($e = 0$). For optimal design, structures $e > 0$ have reduced erosion beneath the structure, increasing stability, protecting it from potential collapse and enhancing dam longevity.

Findings showed that the time to equilibrium is dependent upon the depth of scour (d_s) with deeper d_s taking longer to reach time to equilibrium. Time to reach the depth of scour at equilibrium is affected by discharge and structure design. In Series 1A, the scouring process took longer to reach equilibrium because, as the gap below the structure increased, the effective blockage area decreases, resulting in reduced velocity and a slower scour rate until equilibrium was reached. During high discharge, structures with the base cylinder on the bed become elevated due to the maximum depth of scour occurring beneath them. This affects the channel bathymetry and alters its design and function, which has major implications for the design of engineered woody debris dams.

In real-world scenarios, reducing the risk of woody debris dam failure is crucial. Structures positioned on the bed risk collapse due to scouring underneath. Conversely, structures with an elevated base log experience less scouring, reducing structural failure risk. This result has practical applicability, as elevated structures face less scouring, reducing collapse risk, while bed-positioned structures require regular maintenance due to higher scouring risks. Furthermore, scouring beneath woody debris dams on or close to the bed reduces effective blockage area, increases porosity, and decreases their effectiveness in attenuating peak discharge.

2D simulations successfully obtained bed shear stress spatial distributions and localised velocity values at the start of the flume experiments giving further understanding of their hydraulic behaviour at that time. However, Flood Modeller (FM) poses the limitation that it cannot simulate bathymetric evolution with an erodible bed with structures, and therefore could not simulate scour and deposition extent as shown in the flume experiments. However, FM could solve changes in bed shear stress and higher Shields parameter to infer sediment transport variations, though only for specific time locations. As computational modelling advances, further research using this approach would provide greater understanding of the hydraulic effects of varying woody debris dam designs on bathymetric evolution.

Acknowledgements

My special thanks to Dr. Andrew Crayford, Cardiff University and Professor Roger Falconer for their help and guidance. Thanks also go to Dr. Richard Crowder of Jacobs for his support. Thank you to the reviewers for their feedback.

Disclosure statement

No potential conflict of interest was reported by the authors.

Funding

This paper was conducted as part of The Department for Environment, Food and Rural Affairs (DEFRA) and The Engineering and Physical Sciences Research Council (EPSRC) funded PhD.

Data availability statement

The data associated with this study were stored on institution-managed research storage that is no longer accessible following the conclusion of the project. Full methodological details are provided within the article.

References

Beebe JT. 2000. Flume studies of the effect of perpendicular log obstructions on flow patterns and bed topography. Great Lakes Geographer. 7(1):9–25.

Berenbrock C, Trammer AW. 2008. Simulation of flow, sediment transport, and sediment mobility of the Lower Coeurd'Alene River, Idaho. United States Geological Survey. USGS, Scientific Investigation Report. 2008-5093.

Beschta RL. 1983. The effects of large organic debris upon channel morphology: a flume study. In: Proceedings of the D.B. Simons symposium on erosion and sedimentation. Vol 8-63 to 8-78. Fort Collins, CO: Simons, Li and Associates.

Cherry J, Beschta RL. 1989. Coarse woody debris and channel morphology: a flume study[1]. JAWRA J Am Water Resour Assoc. 25(5):1031–1036. https://doi.org/10.1111/j.1752-1688.1989.tb05417.x

Chiew YM, Melville BW. 1987. Local scour around bridge piers. J Hydraul Res. 25(1):15–26. https://doi.org/10.1080/00221688709499285

Dadson, S. J., Hall, J. W., Murgatroyd, A., Acreman, M., Bates, P., Beven, K., Heathwaite, L., Holden, J., Holman, I. P., Lane, S. N., O'Connell, E., Penning-Rowsell, E., Reynard, N., David Sear, D., Thorne, C., Wilby, R. (2017). A restatement of the natural science evidence concerning catchment-based 'natural' flood management in the UK. Proc Roy Soc A: Math Phys Eng Sci 473:20160706. https://doi.org/10.1098/rspa.2016.0706

Falconer RA. 1986. Mathematical modelling of flow and pollutant transport in rivers, lakes, estuaries and coastal waters. Vol. II. University of Birmingham. 2nd–4th September 1986.

Fredsøe J. 2016. Pipeline–seabed interaction. J Waterway Port Coastal Ocean Eng. 142(6):1–65.

Furnues D. 2023. Modelling woody debris dam form to function to location for flood purposes [PhD thesis]. School of Engineering, Cardiff University.

Gao FP, Yang B, Wu YX, Yan SM. 2006. Steady current induced seabed scour around a vibrating pipeline. Appl Ocean Res. 28:291–298. https://doi.org/10.1016/j.apor.2007.01.004

Jiménez Cisneros BEet al. 2014. Freshwater resources. In: Field C. B., Barros V. R., Dokken D. J., Mach K. J., Mastrandrea M. D., Bilir T. E., Chatterjee M., Ebi K. L., Estrada Y. O., Genova R. C., Girma B., Kissel E. S., Levy A. N., MacCracken S., Mastrandrea P. R., White L.L., editor. Climate change (2014) impacts, adaptation, and vulnerability. Part A: Global and sectoral aspects. Contribution of working group II to the fifth assessment report of the intergovernmental panel on climate change. Cambridge University Press; p 229–269.

Khoshelham K, Elberink SO. 2012. Accuracy and resolution of kinect depth data for indoor mapping applications. Sensors. 12:1437–1454. https://doi.org/10.3390/s120201437

Kovats RSet al. 2014. Europe. In: Climate change 2014: Impacts, adaptation, and vulnerability. Part B: Regional aspects. Contribution of working group II to the fifth assessment report of the intergovernmental panel on climate change. Cambridge University Press; p 1267–1326.

Leakey S, Hewett CJM, Glenis V, Quinn PF. 2020. Modelling the impact of leaky barriers with a 1D Godunov-type scheme for the shallow water equations. Water. 12(2):371. https://doi.org/10.3390/w12020371

Lee JY, Forrest AL, Hardjanto FA, Chai S, Cossu R, Leong ZQ. 2018. Development of current-induced scour beneath elevated subsea pipelines. J Ocean Eng Sci. 3(4):265–281. https://doi.org/10.1016/j.joes.2018.09.001

Li X. 2018. Feature based calibration of a network of kinect sensors [MSc. Thesis]. The University of Western Ontario.

Mankoff KD, Russo TA. 2013. The kinect: a low-cost, high-resolution, short-range 3D camera. Earth Surf Process Landforms. 38:926–936. https://doi.org/10.1002/esp.3332

McParland M. 2021. Modelling the hydraulic and sediment dynamics of leaky barriers in relation to Natural Flood Management [PhD thesis]. University of Liverpool.

Melville BW, Sutherland AJ. 1988. Design method for local scour at bridge piers. J Hydraul Eng. 114(10):1210–1226. https://doi.org/10.1061/(ASCE)0733-9429(1988)114:10(1210)

Ngai Ret al. 2017. Working with natural processes – Appendix 2: Literature review. SC150005. Environment Agency.

Nunnally NR. 1978. Stream renovation: an alternative to channelization. Environ Manage. 2:403–411. https://doi.org/10.1007/BF01872915

Obach LM. 2011. The hydrodynamics of Pool–Riffle sequences with changing Bedform length. Master of Applied Science in Civil Engineering.

Pearson EG. 2020. Modelling the interactions between geomorphological processes and Natural Flood Management [PhD Thesis]. University of Leeds: p 251.

Penna N, Coscarella F, Gaudio R. 2020. Turbulent flow field around horizontal cylinders with scour hole. Water. 12(143):143–118. https://doi.org/10.3390/w12010143

Sankar S. 2015. Turbulent flow in open channel with different froude numbers. In: Xie L, editor. Resources, environment and engineering 11: Proceedings of the 2nd technical congress on resources, environment and engineering (CREE 2015, Hong Kong). Routledge; p 135.

Svoboda CD, Russell K. 2011. Flume analysis of engineered large wood structures for scour development and habitat. In: World environmental and water resources congress. p 2572–2581.

Tammela S, Marttila H, Dey S, Kløve B. 2010. Effect and design of an underminer structure. J Hydraul Res. 48(2):188–196. https://doi.org/10.1080/00221681003704202

Thompson DM, McCarrick CR. 2010. A flume experiment on the effect of constriction shape on the formation of forced pools. Hydrol Earth Syst Sci. 14:1321–1330. https://doi.org/10.5194/hess-14-1321-2010

Whitten DGA, Brooks JRV. 1972. Dictionary of geology. Penguin Books.

Wingfield T, Macdonald N, Peters K, Spees J, Potter K. 2019. Natural flood management: beyond the evidence debate. Area. 51(4):743–751. https://doi.org/10.1111/area.12535

Yang S, Shi B, Guo Y. 2019. Investigation on scour scale of piggyback pipeline under wave conditions. Ocean Eng. 182:196–202. https://doi.org/10.1016/j.oceaneng.2019.04.074